PHYSICAL REVIEW D **96,** 123528 (2017)

Evolution of hydromagnetic turbulence from the electroweak phase transition

Axel Brandenburg,[1,2,3,4] Tina Kahniashvili,[5,6,7,*] Sayan Mandal,[5] Alberto Roper Pol,[1,8] Alexander G. Tevzadze,[9,7] and Tanmay Vachaspati[10]

[1]*Laboratory for Atmospheric and Space Physics, University of Colorado, Boulder, Colorado 80303, USA*
[2]*JILA and Department of Astrophysical and Planetary Sciences, University of Colorado, Boulder, Colorado 80303, USA*
[3]*Nordita, KTH Royal Institute of Technology and Stockholm University, Roslagstullsbacken 23, 10691 Stockholm, Sweden*
[4]*Department of Astronomy, AlbaNova University Center, Stockholm University, 10691 Stockholm, Sweden*
[5]*McWilliams Center for Cosmology and Department of Physics, Carnegie Mellon University, 5000 Forbes Avenue, Pittsburgh, Pennsylvania 15213, USA*
[6]*Department of Physics, Laurentian University, Ramsey Lake Road, Sudbury, Ontario P3E 2C,Canada*
[7]*Abastumani Astrophysical Observatory, Ilia State University, 3-5 Cholokashvili Street, 0194 Tbilisi, Georgia*
[8]*Department of Aerospace Engineering Sciences, University of Colorado, Boulder, Colorado 80303, USA*
[9]*Faculty of Exact and Natural Sciences, Javakhishvili Tbilisi State University, 3 Chavchavadze Avenue, Tbilisi 0179, Georgia*
[10]*Physics Department, Arizona State University, Tempe, Arizona 85287, USA*

(Received 10 November 2017; published 26 December 2017)

We present new simulations of decaying hydromagnetic turbulence for a relativistic equation of state relevant to the early Universe. We compare helical and nonhelical cases either with kinetically or magnetically dominated initial fields. Both kinetic and magnetic initial helicities lead to maximally helical magnetic fields after some time, but with different temporal decay laws. Both are relevant to the early Universe, although no mechanisms have yet been identified that produce magnetic helicity with strengths comparable to the big bang nucleosynthesis limit at scales comparable to the Hubble horizon at the electroweak phase transition. Nonhelical magnetically dominated fields could still produce picoGauss magnetic fields under most optimistic conditions. Only helical magnetic fields can potentially have nanoGauss strengths at scales up to 30 kpc today.

DOI: 10.1103/PhysRevD.96.123528

I. INTRODUCTION

A host of astrophysical observations indicate the presence of coherent magnetic fields with strengths at the microGauss (μG) level from the scale of galaxies to clusters of galaxies [1]. It is thought that such fields may have originated from cosmological or astrophysical seed fields which were subsequently amplified during structure formation, via processes like adiabatic compression and magnetohydrodynamic (MHD) turbulence instabilities [2–4]. The statistical properties of the resulting magnetic field, viz. the amplitude, spectral shape, and the correlation length, depend strongly on the initial conditions, i.e., on the particular generation mechanism.

Primordial magnetic fields can be generated through *causal* processes which include all astrophysical scenarios as well as primordial magnetogenesis occurring after inflation. In all those cases, the correlation length is bounded and limited by the *causal horizon* which is associated with the Hubble horizon scale at the time of magnetic field production [5]. If one accounts for the turbulent magnetic evolution during the expansion of the Universe, the correlation length may reach galactic length scales today [6]. In contrast, Refs. [7,8] assumed that the turbulent evolution is less effective in increasing the magnetic correlation length and obtained a faster decay of magnetic energy.

The evolution of the magnetic field and other observable signatures depend strongly on the magnetic helicity of the initial seed field [9]. A number of astrophysical objects, ranging from stars [10] to jets from active galactic nuclei have detectable magnetic helicity [11]. Usually, the magnetic helicity is initially much less than the maximum possible value, which is given by the product of magnetic energy and the magnetic correlation length. However, the fractional helicity increases due to MHD turbulence. This leads to a maximally helical configuration of the observed fields [12].

If primordial magnetic helicity is detected, it will indicate a statistically significant violation of parity (or mirror symmetry) in the early Universe, and may point towards a resolution to the matter-antimatter asymmetry

*Corresponding author.
tinatin@andrew.cmu.edu

problem [13–16]. To generate causal helical magnetic fields in the early Universe, one requires a fundamental parity violation that affects the outcome of cosmological phase (electroweak or QCD) transitions [17–32].

Assuming that the (comoving) mean energy density of the magnetic field $\mathcal{E}_M \equiv \langle \boldsymbol{B}^2 \rangle/2$, where $\boldsymbol{B}$ is the magnetic field in Lorentz-Heaviside units, depends only on the present day temperature T_0 and fundamental constants such as the Boltzmann constant k_B, the reduced Planck constant $\hbar$, and the speed of light c, one finds, on dimensional grounds,

$$\langle \boldsymbol{B}^2 \rangle/2 \lesssim \epsilon_1 (k_B T_0)^4/(\hbar c)^3, \tag{1}$$

where ϵ_1 is a dimensionless number. For $\epsilon_1 = 1$, this results in a root mean square (rms) field strength of 3×10^{-6} G. (To get the field in Gauss, one has to multiply the Lorentz-Heaviside value by $\sqrt{4\pi}$.) A certain fraction of this magnetic field strength is also what is known as the big bang nucleosynthesis (BBN) bound, which implies that the total energy density budget, in addition to radiation and other relativistic components, should not exceed 10% of the radiation energy density at the moment of BBN. Equation (1) implies that the mean comoving magnetic energy density is determined by today's temperature T_0. On the other hand, today's temperature is set by the photon (radiation) energy density, and the dimensionless quantity ϵ_1 is a ratio between the mean comoving magnetic energy and today's radiation energy densities.

The conserved magnetic helicity per unit volume, i.e., the mean magnetic helicity density[1] is roughly given by $\langle \boldsymbol{B}^2 \rangle \xi_M$, where ξ_M is the magnetic correlation length. As above, assuming that this product depends only on T_0 and the fundamental constants k_B, $\hbar$, and c, one finds [33]

$$\langle \boldsymbol{B}^2 \rangle \xi_M \lesssim \epsilon_2 (k_B T_0)^3/(\hbar c)^2, \tag{2}$$

where ϵ_2 is a dimensionless number. This results in a field strength of 5×10^{-19} G for $\xi_M = 1$ Mpc and $\epsilon_2 = 1$. (For $\xi_M = 10$ kpc, which is more suitable for magnetic fields produced during the electroweak phase transition [6], the corresponding field strength would be 5×10^{-18} G.)

Larger values of $\langle \boldsymbol{B}^2 \rangle \xi_M$ are possible if the underlying physics involves another fundamental constant, for example Newton's constant G. In that case, again just on dimensional grounds, one can write

$$\langle \boldsymbol{B}^2 \rangle \xi_M \lesssim \epsilon_3 (a_\star/a_0)^3 G^{-3/2} \hbar^{-1/2} c^{11/2}, \tag{3}$$

where $a_\star/a_0 = 8 \times 10^{-16}$ is the ratio of the scale factor at the time of magnetic field generation (the electroweak phase transition) to that at the present time. This corresponds to a field strength of 4×10^6 G for $\xi_M = 1$ Mpc and $\epsilon_3 = 1$. Alternatively, of course, geometric means between Eqs. (2) and (3) are conceivable. Of particular interest would be a 2:1 mixing ratio,

$$\langle \boldsymbol{B}^2 \rangle \xi_M \lesssim \epsilon_2^{2/3} \epsilon_3^{1/3} (a_\star/a_0)(k_B T_0)^2 G^{-1/2} \hbar^{-3/2} c^{1/2}, \tag{4}$$

i.e., $10^{-20} \epsilon_2^{2/3} \epsilon_3^{1/3}$ G^2 Mpc, or 10^{-10} G for $\xi_M = 1$ Mpc and $\epsilon_2 = \epsilon_3 = 1$. This mixing ratio corresponds to the magnetic field being at the BBN limit and ξ_M being comparable to the Hubble scale.

The considerations above do not allow us to predict the maximum available magnetic helicity unless some physical mechanism is identified. In the case of the chiral magnetic effect [20,31], for example, Newton's constant does not enter, and so Eq. (2) does impose a rather stringent constraint. However, if stronger magnetic helicities are to be produced by some as yet unknown mechanism [34], this should allow us to identify a nonvanishing mixing ratio between Eqs. (2) and (3). The ratio 2:1 is physically appealing, but by no means the only possible choice. Note, however, that the 2:1 ratio is also being reflected in the magnetogenesis scenario with a strong charge-parity (CP) violation. One such option is presented by the scenario of Ref. [22], in which maximal helicity is produced through Chern-Simons CP violation leading to magnetic fields correlated on 100 kpc scales.

In this paper we focus on magnetogenesis mechanisms during the electroweak phase transition, as proposed in Refs. [17,18,23,28,29], assuming that the electroweak phase transition is strongly first order. Our main goal is to study the dynamical evolution of the generated magnetic field during the expansion of the Universe and estimate if it can serve as the initial seed for the observed magnetic fields in galaxies and clusters.

We will determine the evolution of the magnetic field from the electroweak epoch until the epoch of recombination. We can evolve the magnetic field from recombination to the present epoch by using the fact that the primordial plasma is neutral after recombination and the free MHD decay stops, so the comoving amplitude, spectral shape, and helicity of the magnetic field stay unchanged until large-scale structure formation and reionization. In the following, we neglect further nonlinear evolution of the magnetic field during large-scale structure formation and reionization.

Since the first order phase transition proceeds via bubble nucleation and subsequent collisions of these bubbles [35], there is stirring of the plasma at high Reynolds numbers and consequent generation of turbulence. This occurs in addition to the magnetic fields that are produced. Correspondingly, the turbulent motions can be (i) magnetically dominant, (ii) hydrodynamically dominant (i.e., magnetically subdominant), or (iii) have approximate equipartition between magnetic and kinetic energies. We address all these cases separately. Most of the earlier investigations have employed magnetically dominated

[1]In the following we talk about magnetic helicity and omit the specification to mean helicity density for simplicity.

turbulence [9,36]. Recently, for the first time, we have considered a magnetically subdominant case, but with initial kinetic helicity [37].[2]

In Sec. II we briefly review the electroweak phase transition magnetogenesis, and we determine the initial conditions for further evolution of the magnetic field. We study the evolution of MHD turbulence under the initial conditions presented in Sec. II using direct numerical simulations (DNS) in Secs. III and IV. We discuss our results and conclude in Secs. V and VI, respectively. From now on, we use natural ($\hbar = k_B = c = 1$) Lorentz-Heaviside units. So there are no factors of 4π in the Maxwell equations and the magnetic energy density is $\boldsymbol{B}^2/2$. Unless specified, t denotes the conformal time, $dt = d\tau/a(\tau)$ [with τ the physical time, and $a = a(\tau)$ the scale factor)]. We normalize the scale factor to be unity today, i.e., $a_0 = a(\tau = \tau_0) = 1$.

The expansion of the Universe can be eliminated from the relativistic MHD equations through the use of suitably rescaled (comoving) quantities [38]. For example, we use the comoving value for the magnetic field, i.e., $\boldsymbol{B} \to a^2\boldsymbol{B}$, which also reflects magnetic flux conservation for a *frozen-in* magnetic field in the expanding Universe. To avoid confusion $\tilde{\boldsymbol{B}}$ will denote the physical magnetic field.

II. ELECTROWEAK PHASE TRANSITION MAGNETOGENESIS

We investigate the scenario where a cosmological magnetic field is generated during baryogenesis at the electroweak phase transition at conformal time $t = t_\star$ (that corresponds to the temperature $T_\star$). The phase transition is assumed to be strongly first order, and the magnetic field is produced by anomalous baryon number violation as described in Refs. [17,23,28–30,39]. The magnetic field immediately after production is assumed to be a statistically homogeneous and isotropic, Gaussian-distributed vector field, and is described in terms of the equal time correlation function [40],

$$\langle B_i^*(\boldsymbol{k},t)B_j(\boldsymbol{k}',t)\rangle = (2\pi)^3\delta^3(\boldsymbol{k}-\boldsymbol{k}')F_{ij}(\boldsymbol{k},t), \quad (5)$$

where $\boldsymbol{B}(\boldsymbol{k},t)$ is the Fourier transform[3] of $\boldsymbol{B}(\boldsymbol{x},t)$. The correlation function $F_{ij}(\boldsymbol{k},t)$ has nonhelical (symmetric) and helical (antisymmetric) components,

$$\frac{F_{ij}(\boldsymbol{k},t)}{(2\pi)^3} = P_{ij}(\hat{\boldsymbol{k}})\frac{E_{\rm M}(k,t)}{4\pi k^2} + i\epsilon_{ijl}k_l\frac{H_{\rm M}(k,t)}{8\pi k^2}, \quad (6)$$

where $P_{ij}(\hat{\boldsymbol{k}}) \equiv \delta_{ij} - \hat{k}_i\hat{k}_j$ is the projection operator that projects any vector in the direction orthogonal to $\hat{\boldsymbol{k}}$ and ensures the solenoidal nature of the magnetic field.

Note that the form of the correlation function in Eq. (5) assumes statistical isotropy—rotational symmetry is preserved, while mirror (parity) symmetry is broken by the helical component. Assuming that the real space two-point correlation function $\langle \boldsymbol{B}(\boldsymbol{x})\boldsymbol{B}(\boldsymbol{x}+r)\rangle$ vanishes for $|r| \to \infty$, the form of the correlator $F_{ij}(k,t)$ in Eq. (6) is strictly valid only if the spectrum $E_{\rm M}(k,t)$ falls off faster than k^2 as $k \to 0$ and fixed time t [40].[4]

A. Modeling primordial magnetic field

Motivated by electroweak baryogenesis, extensions of the standard model, in which the electroweak phase transition is strongly first order, have been considered (recently in [42]). The models include the standard model with an extra singlet [43], the two-Higgs doublet model [44], and the Next-to-Minimal Supersymmetric Standard Model (NMSSM) [44]. For our work we will assume that there is a strong first order phase transition at the electroweak epoch [45]. The phase transition then proceeds by bubble nucleation and growth, and since it is a strong first order transition, the typical bubble size at percolation can be large, perhaps even of the order of $\tau_\star$. During the phase transition, there are baryon number violating particle interactions in the medium that also generate helical magnetic fields as a by-product [23,28,30]. Far outside the bubbles, where the electroweak symmetry is unbroken, we expect the magnetic fields to be in thermal equilibrium. Inside the bubbles, the electroweak symmetry is broken, the weak gauge fields are massive, and baryon number violation is suppressed. Then there is no magnetic field production within the bubbles. However, any magnetic field that is generated just outside the bubble walls gets trapped once the bubble expands further and this magnetic field can survive. Once the phase transition is over, space is filled with helical magnetic fields that were generated by baryon number violation occurring near the bubble walls.

[2]The generation of kinetic helicity during parity or chirality violating electroweak phase transitions can be expected since the interaction strengths of the left- and right-handed particles are different.

[3]We use the following convention for the forward and inverse Fourier transforms of an arbitrary vector field $\boldsymbol{A}(\boldsymbol{x})$

$$A_i(\boldsymbol{k}) = \int d^3x A_i(\boldsymbol{x})e^{i\boldsymbol{k}\cdot\boldsymbol{x}}, A_i(\boldsymbol{x}) = \int \frac{d^3k}{(2\pi)^3}A_i(\boldsymbol{k})e^{-i\boldsymbol{k}\cdot\boldsymbol{x}}.$$

[4]The *causal* magnetogenesis mechanisms considered here do not include magnetic fields generated during cosmological inflation in which a scale invariant spectrum with $E_{\rm M}(k) \propto k^{-1}$ is produced. A scale-invariant spectrum has an *unlimited* correlation length scale and cannot be generated by causal processes during cosmological phase transitions. Following Ref. [40], the requirement that the correlation function in Eq. (5) be analytic for $k \to 0$ leads to $E_{\rm M}(k) \propto k^4$ (the so called Batchelor spectrum). A similar shape has been discussed in Ref. [41] in which the authors argued that the magnetic field should have strictly vanishing spatial correlation on length scales larger than the cosmological horizon scale and then should fall off faster than k^4 (instead of k^2 for white noise) to be divergence free.

Baryon number violating processes will sometimes produce baryons and sometimes anti-baryons. *CP* violating terms in the model will lead to a slight excess of baryons. In terms of magnetic fields, this means that both left- and right-handed magnetic fields will be produced but there will be an excess of left-handed helicity.

A strong first order electroweak phase transition is also likely to produce turbulence in the cosmological medium [35]. Particles of the cosmological medium are massless outside the bubbles and massive within. Thus the bubble wall interacts with the particles and pushes the medium in front of it in what is described as a snowplow effect. The typical turbulence eddy turnover velocity is given by [35]

$$u_T = \sqrt{\frac{\tilde{\kappa}\tilde{\alpha}}{\frac{4}{3}+\tilde{\kappa}\tilde{\alpha}}}, \tag{7}$$

where $\tilde{\alpha}$ denotes the ratio of the false vacuum energy density (latent heat) and the plasma thermal energy density, and characterizes the strength of the phase transition; $\tilde{\kappa}$ is an efficiency parameter that is determined by $\tilde{\alpha}$ and has to be computed numerically [46],

$$\tilde{\kappa}(\tilde{\alpha}) \simeq \frac{1}{1+0.715\tilde{\alpha}}\left[0.715\tilde{\alpha}+\frac{4}{27}\sqrt{\frac{3\tilde{\alpha}}{2}}\right]. \tag{8}$$

A strong phase transition is described by $\tilde{\alpha} \gtrsim 1$ and a weak phase transition has $\tilde{\alpha} \ll 1$.

Another important parameter that characterizes the forcing stage of turbulence is the duration of the phase transition described by a parameter $\tilde{\beta}$, which is the rate of time variation of the nucleation rate itself computed at the phase transition time $\tau_\star$. Thus, $\tilde{\beta}^{-1}$ gives a time scale during which the whole Universe is converted to the true vacuum phase (typically $\tilde{\beta} \gg H_\star$) [47].

An outcome of the DNS of the magnetic field generation process is that the initial magnetic field spectrum is peaked at a scale that corresponds to the size of the bubbles at percolation. Hence, for a strong first order phase transition, the initial magnetic field can be correlated on cosmological scales. Let us denote this initial (physical) correlation length by $l_\star$ and define the dimensionless parameter $\gamma_\star = l_\star H_\star$, which we will take as a free parameter in the interval $10^{-4} < \gamma_\star < 0.1$ (it is commonly assumed that for a first order electroweak phase transition $\gamma \simeq 0.01$ [48,49]). It is of interest to evaluate the comoving value of the Hubble length scale at the electroweak phase transition. We have already stated $H_\star^{-1} \approx 1$ cm. Then, the comoving value, denoted $\lambda_{H_\star}$, is given by

$$\lambda_{H_\star} \equiv \frac{a_0}{a_\star}H_\star^{-1} = 5.8\times10^{-10}\ \mathrm{Mpc}\left(\frac{100\ \mathrm{GeV}}{T_\star}\right)\left(\frac{100}{g_\star}\right)^{1/6}, \tag{9}$$

where the subscripts $\star$ and 0 denote, respectively, the epoch of the magnetic field generation and the present epoch; $g_\star$ is the number of relativistic degrees of freedom in the medium at the electroweak epoch, and we have used the time-temperature relation

$$\frac{a_\star}{a_0} \simeq 8\times10^{-16}\left(\frac{100\ \mathrm{GeV}}{T_\star}\right)\left(\frac{100}{g_\star}\right)^{1/3}. \tag{10}$$

The numerical value of $\lambda_{H\star} \approx 6\times10^{-4}$ pc is much smaller than the current horizon scale $\sim$1 Gpc, and without significant growth, would not be an interesting scale for astrophysics. However, it is known that turbulent MHD evolution of helical magnetic fields allows for an inverse cascade that can lead to a significantly larger coherence scale, even larger than $\sim$10 kpc [6,28,38]. This is also seen in the results of our DNS.

An important quantity associated with the primordial magnetic field is its total energy density at the moment of generation, $\rho_{\mathrm{M}\star}$. Since the frozen-in (physical) magnetic field amplitudes scale with the expansion of the Universe as $\tilde{B} \sim a^{-2}$, the magnetic energy density scales like *radiation* if dissipation and/or amplification processes are ignored. So the ratio of the magnetic and radiation energy densities stays constant during the expansion of the Universe. BBN bounds the radiationlike energy density during BBN, and *only* $\sim$10% of the ordinary radiation energy density can be additionally present in the Universe in the form of another relativistic component [50]. In particular, during the radiation-dominated epoch, neglecting the presence of any additional relativistic components, the Friedman equation in the flat Friedmann-Lemaître-Robertson-Walker (FLRW) metric, reads $3H^2 = 8\pi G\rho_{\mathrm{R}}$ where ρ_{R} denotes the (physical) radiation energy density. The expansion rate (H) can be limited by the rate of nucleosynthesis (that is bounded by the abundance of light elements in the Universe). At the electroweak epoch, the radiation energy density is given by $\rho_R(t_\star) = \pi g_\star T_\star^4/30$, where $g_\star$ is the number of degrees of freedom at the temperature $T_\star$. Applying the BBN bound that $\rho_{\mathrm{M}}(t_\star)/\rho_R(t_\star) \le 0.1$ (with $\rho_{\mathrm{M}} = \tilde{B}^2/2$) and assuming a frozen-in magnetic field ($\tilde{B} \propto a^{-2}$), the *comoving* magnetic field strength can be no larger than $8.4\times10^{-7}(100/g)^{1/6}$ G $\sim 1\,\mu$G,[5] which agrees well with the dimensional argument given in Sec. I. In our DNS we take

$$b_\star \equiv \sqrt{\frac{\rho_{\mathrm{M}\star}}{0.1\rho_{R\star}}} \approx \frac{B_\star}{\mu\mathrm{G}} \lesssim 1 \tag{11}$$

to be a free parameter of the model.

We define the Alfvén velocity associated with the magnetic field, $\boldsymbol{v}_{\mathrm{A}} = \boldsymbol{B}/\sqrt{w}$, where $w = \rho + p$ is the

[5]Here we have assumed that the number of relativistic degrees of freedom, g, is unchanged from the electroweak phase transition until BBN.

specific enthalpy for an ultrarelativistic gas with density ρ and pressure p. The mean normalized magnetic and kinetic energy densities per unit mass are $\langle \boldsymbol{v}_{\rm A}^2(t)\rangle/2$ and $\langle \boldsymbol{u}^2(t)\rangle/2$, with $\boldsymbol{u}(\boldsymbol{x},t)$ denoting the velocity and angular brackets denote ensemble averaging. If the physical magnetic field scales as a^{-2} with the expansion of the Universe, the Alfvén velocity $\boldsymbol{v}_{\rm A}(\boldsymbol{x},t)$ is time independent, and thus does not require rescaling to the comoving quantity. At this point $\boldsymbol{v}_{\rm A}(\boldsymbol{x},t)$ is fully determined by the initial value of the magnetic field, i.e., $v_{\rm A}(\boldsymbol{x},t) = v_{\rm A\star}(\boldsymbol{x}) \equiv v_{\rm A}(\boldsymbol{x}, t = t_\star)$.

Owing to the presence of hydromagnetic turbulence, the magnetic field evolution can be described by a simple power law, $B(\boldsymbol{x},t) = B_\star(\boldsymbol{x})(t/t_\star)^{n_E/2}$, where n_E characterizes the scaling of the decay of mean magnetic energy density $\mathcal{E}_{\rm M}(t) = \langle \boldsymbol{B}^2(\boldsymbol{x},t)\rangle/2$, which be written in terms of the magnetic energy spectrum $E_{\rm M}(k,t)$ as

$$\mathcal{E}_{\rm M}(t) = \int dk E_{\rm M}(k,t), \tag{12}$$

while the magnetic helicity,[6] defined as $\mathcal{H}_{\rm M} = \langle \boldsymbol{A}\cdot\boldsymbol{B}\rangle$ with $\boldsymbol{B} = \boldsymbol{\nabla}\times\boldsymbol{A}$, and can be computed through the magnetic helicity spectrum as

$$\mathcal{H}_{\rm M}(t) = \int dk H_{\rm M}(k,t). \tag{13}$$

The magnetic correlation length is defined as

$$\xi_{\rm M}(t) = \frac{\int dk k^{-1} E_{\rm M}(k,t)}{\mathcal{E}_{\rm M}(t)}. \tag{14}$$

Assuming that this integral converges, the realizability condition can be written as

$$2E_{\rm M}(k,\tau) \geq k|H_{\rm M}(k,\tau)|. \tag{15}$$

This is a consequence of the Cauchy-Bunyakovsky-Schwarz inequality and implies that the magnetic energy cannot decay faster than the helicity [51]. On integration, the realizability condition gives [52,53]

$$2\xi_{\rm M}(\tau)\mathcal{E}_{\rm M}(\tau) \geq |\mathcal{H}_{\rm M}(\tau)| \tag{16}$$

and implies that the *maximal* helicity is $2\int_0^\infty dk k^{-1} E_{\rm M}(k)$.

Alternately, one can say that there is a lower bound on $\xi_{\rm M}$ given by,

$$\xi_{\rm M}^{\rm min}(t) \equiv \frac{\mathcal{H}_{\rm M}(t)}{2\mathcal{E}_{\rm M}(t)}. \tag{17}$$

The realizability condition then implies $\xi_{\rm M}^{\rm min} \leq \xi_{\rm M}$. This allows us to define the fractional magnetic helicity as

$$\epsilon_{\rm M}(t) = \frac{\xi_{\rm M}^{\rm min}(t)}{\xi_{\rm M}(t)} = \frac{\mathcal{H}_{\rm M}(t)}{2\xi_{\rm M}(t)\mathcal{E}_{\rm M}(t)} \leq 1. \tag{18}$$

Its initial value is related to a parameter $\sigma_{\rm M\star}$ that will be defined below and will serve as a free parameter.

Another free parameter in our considerations is the initial velocity, $u_\star$. Applying the BBN bound on the kinetic energy density, $\mathcal{E}_K(t)$, which should be less than 10% of the radiation energy density (i.e., $\leq 0.1\rho_{\rm R}$), we obtain that $u_\star \leq 0.4$ if decay and/or amplification of the velocity field during turbulence is neglected (the initial velocity field is assumed to be unchanged from the electroweak epoch until the BBN epoch).

III. MAGNETIC FIELD EVOLUTION

We follow the evolution of fields from the epoch right after magnetogenesis up to the recombination epoch. We are interested in the evolution of the magnetic energy density $\mathcal{E}_{\rm M}(t)$, which determines the rms value of the magnetic field, $B_{\rm rms}(t) = \sqrt{2\mathcal{E}_{\rm M}(t)}$, and the correlation length $\xi_{\rm M}(t)$. For a partially helical magnetic field we study the redistribution of helical structures at large scales, and estimate the time scale during which the field might become fully helical. We also study the evolution of the velocity field.

A. Direct numerical simulations

We solve the equations for the logarithmic total energy density $\ln\rho$, the velocity $\boldsymbol{u}$, and the magnetic vector potential $\boldsymbol{A}$, in the form [38]

$$\frac{\partial \ln\rho}{\partial t} = -\frac{4}{3}(\boldsymbol{\nabla}\cdot\boldsymbol{u} + \boldsymbol{u}\cdot\boldsymbol{\nabla}\ln\rho) + \frac{1}{\rho}[\boldsymbol{u}\cdot(\boldsymbol{J}\times\boldsymbol{B}) + \eta\boldsymbol{J}^2], \tag{19}$$

$$\frac{{\rm D}\boldsymbol{u}}{{\rm D}t} = \frac{\boldsymbol{u}}{3}(\boldsymbol{\nabla}\cdot\boldsymbol{u} + \boldsymbol{u}\cdot\boldsymbol{\nabla}\ln\rho) - \frac{\boldsymbol{u}}{\rho}[\boldsymbol{u}\cdot(\boldsymbol{J}\times\boldsymbol{B}) + \eta\boldsymbol{J}^2] - \frac{1}{4}\boldsymbol{\nabla}\ln\rho + \frac{3}{4\rho}\boldsymbol{J}\times\boldsymbol{B} + \frac{2}{\rho}\boldsymbol{\nabla}\cdot(\rho\nu\mathsf{S}), \tag{20}$$

$$\frac{\partial \boldsymbol{B}}{\partial t} = \nabla\times(\boldsymbol{u}\times\boldsymbol{B} - \eta\boldsymbol{J}), \tag{21}$$

where $\boldsymbol{B} = \nabla\times\boldsymbol{A}$ and ${\rm D}/{\rm D}t = \partial/\partial t + \boldsymbol{u}\cdot\boldsymbol{\nabla}$ is the advective derivative, $\boldsymbol{f}_{\rm visc} = \nu(\nabla^2\boldsymbol{u} + \frac{1}{3}\boldsymbol{\nabla}\boldsymbol{\nabla}\cdot\boldsymbol{u} + \boldsymbol{G})$ is the viscous force in the compressible case with $G_i = 2\mathsf{S}_{ij}\nabla_j\ln\nu\rho$ as well as $\mathsf{S}_{ij} = \frac{1}{2}(u_{i,j} + u_{j,i}) - \frac{1}{3}\delta_{ij}u_{k,k}$ being the trace-free rate of strain tensor. The pressure is given by $p = \rho c_{\rm s}^2$, where $c_{\rm s} = 1/\sqrt{3}$ is the sound speed for an ultrarelativistic gas. Furthermore, $\boldsymbol{J} = \boldsymbol{\nabla}\times\boldsymbol{B}$ is the current density. In Appendix A we discuss the main difference from the usual MHD equations for a nonrelativistic isothermal gas.

[6] $\mathcal{H}_{\rm M}(t)$ is distinct from the *current helicity* $\mathcal{H}_{\rm C}(t) = \langle \boldsymbol{B}\cdot\boldsymbol{\nabla}\times\boldsymbol{B}\rangle$; the current helicity spectrum is $H_{\rm C}(k,t) \equiv k^2 H_{\rm M}(k,t)$.

In contrast to some of our previous studies [6,12,54] in which the initial magnetic energy spectrum was assumed to be a δ-function (the magnetic field energy density has been injected at a given wave number), in the present work we assume the initial spectra to be given by $E_{\rm M}(k,t_\star)$ and $H_{\rm M}(k,t_\star)$. We also use different conditions for the velocity field, including the magnetically subdominant case and equipartition with the magnetic field. The magnetically dominant case has been studied previously, see [55] and references therein, but the magnetically subdominant and equipartition cases have not been studied. In particular, the cases of kinetically dominant and equipartition MHD decay were presented for the first time in a recent publication [37] by the present authors. The application to cosmology is discussed below.

We allow ν and η to be time-dependent; see Ref. [37] for details. This is done to address the problem that ν and η are very small in the early Universe, but are also subject to numerical limitations in that they cannot be too small, especially at early times when the velocities are still large. We take advantage of the fact that a self-similar evolution is possible by allowing ν and η to vary as

$$\nu(t)=\nu_\star \max(t,t_\star)^r, \tag{22}$$

where $r=(1-\alpha)/(3+\alpha)$ [56] depends on the initial power law slope α, and $t_\star$ is the minimal time after which these coefficients are allowed to be time-dependent. For $\alpha=2$ we have $r=-0.20$, whereas for $\alpha=4$ we have $r=-0.43$, so $\nu(t)$ decreases with time in both cases. We take different values of $\nu_\star$, depending on the value of α. In all cases with $\alpha=2$ we use $\nu_\star=10^{-6}$, while in all cases with $\alpha=4$ we use $\nu_\star=10^{-5}$. We adopt the same initial values for η, i.e., $\eta_\star=\nu_\star$.

For our DNS we use the Pencil Code (https://github.com/pencil-code) which is a public MHD code that is particularly well suited for simulating turbulence. We consider a cubic domain of size L^3, so the smallest wave number in the domain is $k_1=2\pi/L$. The numerical resolution is 1152^3 meshpoints in all the cases presented below.

B. Initial condition

In practice, we construct the initial condition for the magnetic vector potential $\boldsymbol{A}(\boldsymbol{x})$ from a random δ-correlated three-dimensional vector field in real space. It has therefore a k^2 spectrum. We transform this field into Fourier space and construct the magnetic field, $\boldsymbol{B}(\boldsymbol{k})=i\boldsymbol{k}\times\boldsymbol{A}(\boldsymbol{k})$. We then scale the magnetic field by functions of k such that it has the desired *initial* spectrum, apply the projection operator $P_{ij}=\delta_{ij}-\hat{k}_i\hat{k}_j$ (to ensure a divergence free magnetic field),

$$B_i(\boldsymbol{k})=B_\star[P_{ij}(\boldsymbol{k})-{\rm i}\sigma_{\rm M}\epsilon_{ijl}\hat{k}_l]g_j(\boldsymbol{k})S(k), \tag{23}$$

where $g_j(\boldsymbol{k})$ is the Fourier transform of a δ-correlated vector field in three dimensions with Gaussian fluctuations, i.e., $g_i(\boldsymbol{x})g_j(\boldsymbol{x}')=\delta_{ij}\delta^3(\boldsymbol{x}-\boldsymbol{x}')$, k_0 is the initial wave number of the energy-carrying eddies and $S(k)$ determines the spectral shape with

$$S(k)=\frac{k_0^{-3/2}(k/k_0)^{\alpha/2-1}\exp[-\mathcal{G}(k^2/k_0^2-1)]}{[1+(k/k_0)^{2(\alpha+5/3)}]^{1/4}}, \tag{24}$$

where $\mathcal{G}=0$ in most cases, and $\mathcal{G}=1$ in some special cases where the initial power is more strongly concentrated around $k=k_0$. This results in a random magnetic field with the desired magnetic energy and helicity spectra and obeys

$$\frac{kH_{\rm M}(k,t_\star)}{2E_{\rm M}(k,t_\star)}=\frac{2\sigma_{\rm M}}{1+\sigma_{\rm M}^2}\equiv\epsilon_{\rm M}. \tag{25}$$

A similar scheme allows us to generate the velocity field,

$$u_i(\boldsymbol{k})=u_\star[P_{ij}(\boldsymbol{k})-{\rm i}\sigma_{\rm K}\epsilon_{ijl}\hat{k}_l]g_j(\boldsymbol{k})S(k). \tag{26}$$

These initial condition are implemented as part of the Pencil Code.

We now consider possible initial conditions in a cosmological scenario, where we have in mind magnetic fields generated at the electroweak phase transition. In the standard model, the electroweak phase transition is of second order and CP violation is very weak. However, we also know that the standard model is incomplete, most convincingly because of the observed nonvanishing neutrino masses. In addition, the standard model does not contain a candidate for cosmological dark matter. Neither does it successfully explain the observed baryon asymmetry of the Universe. Hence it is almost certain that there is fundamental physics beyond the standard model.

The exact nature of what lies beyond the standard model is unclear. Yet we expect beyond-standard-model (BSM) physics to explain neutrino masses and contain a suitable dark matter candidate and also have a successful baryogenesis mechanism. The requirement of baryogenesis points to some general features essential to BSM as first outlined by Sakharov [57]: the model should have strong departures from thermal equilibrium and should contain significant violations of charge conjugation (C) symmetry, CP conjugation symmetry, and baryon number.

In the present context, it is possible that strong departures from thermal equilibrium might occur during strong first order phase transitions, in which case the cosmological medium could become turbulent. Thus we would like to include fluid kinetic energy as an initial condition. Electroweak symmetry breaking also leads to the production of magnetic fields [17]. In addition, baryon number violating processes lead to the generation of helical magnetic fields [23,28]. If there is significant violation of C and CP, helicity might be large. One may also expect

C and CP violation to leak into the kinetic motion, in which case the initial conditions would have nonvanishing kinetic helicity.

To keep the discussion as general as possible we consider three different cases for the initial conditions: (i) magnetically dominant turbulence, (ii) kinetically dominant turbulence, and (iii) equipartition between magnetic and kinetic energy densities. In every case, there are several parameters that we have to choose that quantify the magnetic and kinetic energy and helicity spectra such as $B_\star$,[7] $u_\star$, $\sigma_{\rm K}$, and $\sigma_{\rm M}$, defined in Sec. II A. In addition, it is assumed that the phase transition leads to a peak in the spectra at some fraction, $\gamma_\star$, of the Hubble scale. For example, $\gamma_\star$ will depend on the bubble size at percolation in the case of a first order phase transition. The resulting magnetic field values are given for several choices of the parameters.

An important control parameter is the initial ratio of the normalized rms magnetic field (or Alfvén velocity) and rms velocity defined as

$$Q_\star = B_\star/(\rho_\star^{1/2} u_\star). \tag{27}$$

In this work, we consider the values 10, 1, and 0.1, corresponding to magnetically dominant, equipartition, and magnetically subdominant cases. We also consider the time-dependent quantity $Q(t) = v_{\rm A}/u_{\rm rms}$, and list, in particular, the value at the last time, $Q_{\rm e} = Q(t_{\rm e})$. Furthermore, we quote the Reynolds number, ${\rm Re} = u_{\rm rms}\xi_{\rm M}/\nu$, at $t = t_{\rm e}$.

1. Magnetically dominant turbulence

For magnetically dominant turbulence we assume that the velocity field is small initially. The magnetic energy spectrum must satisfy the causality requirements, i.e., the magnetic field two point correlation function $\langle B_i(\mathbf{x}) B_j(\mathbf{x}+\mathbf{r})\rangle \equiv \mathcal{B}_{ij}(r) \to 0$ for $r \geq \xi_{\rm M}$, where $\xi_{\rm M}$ is the magnetic correlation length with its maximal value being given by the comoving Hubble horizon radius, and we have used the isotropy condition, $\mathcal{B}_{ij}(\mathbf{r}) = \mathcal{B}_{ij}(|\mathbf{r}|)$. The causality condition requires that $E_{\rm M}(k, t_\star) \propto k^\alpha$ for $k \to 0$ together with the requirement that $F_{ij}(\mathbf{k})$ is analytical for a solenoidal magnetic field (divergence-free condition $\boldsymbol{\nabla}\cdot\boldsymbol{B} = 0$). This leads to $\alpha \geq 4$ [41]; in practice, one finds the Batchelor spectrum with $\alpha = 4$.

The initial peak position of the magnetic energy spectrum is determined by the phase transition bubble size (i.e., the $\gamma_\star$-parameter). The ratio between the magnetic and kinetic energies at the initial moment is a large number $\mathcal{E}_{\rm M}(t_\star)/\mathcal{E}_{\rm K}(t_\star) \gg 1$, and at all wave numbers k the magnetic energy spectrum is dominant, $E_{\rm M}(k, t_\star) \gg E_{\rm K}(k, t_\star)$. This class of initial conditions is realized in most baryogenesis mechanisms during cosmological phase transitions. It can be also applied when the magnetic field was generated at earlier epochs and undergoes coupling with primordial plasma within the Hubble horizon.

[7]Equivalently we can use $b_\star$; see Eq. (11). Note that $b_\star = 1$ corresponds to the case with maximal magnetic field strength allowed by BBN.

2. Kinetically dominant turbulence

In the case of kinetically dominant turbulence, the initial Alfvén velocity is negligibly small compared to the turbulence turnover velocity; i.e., the magnetic energy density is negligibly small compared to the kinetic energy density, $\mathcal{E}_{\rm M}(t_\star) \ll \mathcal{E}_{\rm K}(t_\star)$, and at all wave numbers k the magnetic energy spectrum is subdominant, $E_{\rm M}(k, t_\star) \ll E_{\rm K}(k, t_\star)$. This class of initial conditions can be realized for a strong first order phase transition when the turbulent turnover velocity $u_T(t_\star) \simeq 0.3$, which is a consequence of high enough values for $\tilde{\alpha}$ and $\tilde{\kappa}$ parameters. This agrees with the BBN bound on the relativistic energy density; see Sec. II. The initial kinetic energy spectrum can be approximated by a white noise spectrum with $E_{\rm K}(k, t_\star) \propto k^2$ (which ensures the causality requirement) or by the Batchelor spectrum $E_{\rm K}(k, t_\star) \propto k^4$ (which ensures the causality and divergence-free requirements). Interestingly in the latter case the initially solenoidal velocity field acquires a longitudinal structure through the interaction with the magnetic field, as will be discussed below. In addition we study the evolution of a magnetic field that has initially a white noise spectrum.

3. The Case of Equipartition

The case of equipartition between magnetic and kinetic energy spectra $\mathcal{E}_{\rm M}(t_\star) \simeq \mathcal{E}_{\rm K}(t_\star)$ is hard to realize in the early Universe and requires very specific physical conditions during phase transitions. We study this case for completeness.

C. Simulation parameters and analysis tools

We compute magnetic and kinetic energy spectra, $E_{\rm M}(k, t)$ and $E_{\rm K}(k, t)$, respectively, and evaluate corresponding magnetic and kinetic correlation lengths using Eq. (14). We define a time-dependent Reynolds number, ${\rm Re} = u_{\rm rms}\xi_{\rm M}/\nu$, and quote approximate values characteristic of the late time evolution.

As demonstrated earlier [55], $E_i(k, t)$ with $i = {\rm M}$ and K can be collapsed onto a function $\phi_i(\kappa)$ of a single argument $\kappa = k\xi_i(t)$ via

$$E_i(k, t) = \xi_i^{-\beta_i}\phi_i(k\xi_i), \tag{28}$$

where β_i quantifies the decay of the spectral energy around the wave number $k = \xi_i^{-1}$, which itself decreases approximately like a power law with $\xi_i(t) \propto t^{q_i}$, where q_i is a scaling exponent. Since $\mathcal{E}_i(t) = \int E_i(k, t)dk$, it also decays like a power law with $\mathcal{E}_i(t) \propto t^{-p_i}$, where

$$p_i = (\beta_i + 1)q_i. \tag{29}$$

The values of β_i are believed to depend on the physics that governs a particular case [55].

It is convenient to define and plot instantaneous scaling exponents as $p_i(t) = d\ln\mathcal{E}_i/dt$ versus $q_i(t) = d\ln\xi_i/dt$ for $i = \mathrm{M}$ and K and discuss the evolution of the point

$$\boldsymbol{P}_i = (p_i, q_i) \tag{30}$$

in the pq diagram. Solutions that obey invariance under rescaling [55,56],

$$k \to k'\ell \quad \text{and} \quad t \to t'\ell^{1/q_i}, \tag{31}$$

all lie on the line $p_i = 2(1 - q_i)$ in this diagram. The functions $\phi_i(\kappa)$ are universal functions for given β_i and thus q_i. If that is the case, then $q_i = 2/(\beta_i + 3)$.

We are particularly interested in the possibility of an inverse cascade, which means that the magnetic energy increases at small wave numbers, even though the total energy decreases. This implies that

$$s_i \equiv \partial\ln E_i(k,t)/\partial\ln t > 0 \quad \text{for } k \ll \xi_i(t)^{-1}. \tag{32}$$

At small $\kappa = k\xi_i(t)$, we have $\phi_i(\kappa) \propto \kappa^{\alpha}$, and therefore

$$s_i = (\alpha_i - \beta_i)q_i, \tag{33}$$

which implies that large initial slopes (e.g., $\alpha = 4$) and small values of β, e.g., when the decay is governed by the conservation of magnetic helicity ($\beta = 0$) or the mean squared vector potential ($\beta = 1$) will lead to an inverse cascade, but not when $\beta \geq 2$ [55].

IV. RESULTS

A. Batchelor spectrum and no helicity

We begin by comparing the evolution of initially nonhelical velocity and magnetic fields for $Q_\star = 10$, 1, and 0.1, corresponding to Runs A–C; see Figs. 1–3 and Table I. In all three cases, we plot $E_i(k,t)$ at selected times, normalized by the initial Alfvén time $t_{\mathrm{A}\star}$. We also show the evolution of $\mathcal{E}_i(t)$ and ξ_i, as well as a parametric representation of the instantaneous scaling exponents $p_i(t)$ versus $q_i(t)$ for $i = \mathrm{M}$ and K (pq diagram). In all three cases (Runs A, B, and C), there is inverse energy transfer at small k, which is in agreement with Eq. (33).

Remarkably, Runs A and B are rather similar at later times, i.e., for $t/t_{\mathrm{A}\star} \gtrsim 10$, where $Q(t) \approx 10$, which agrees with the initial value $Q_\star = 10$ for Run A, but not with that of Run B, where the initial ratio was unity. The resulting values of $p_{\mathrm{M}} \approx 1$ are similar to those obtained earlier from an initial condition obtained from a run that was driven for a short time with a monochromatic magnetic forcing function [58], which is marked in Table I by BKT, where β turned

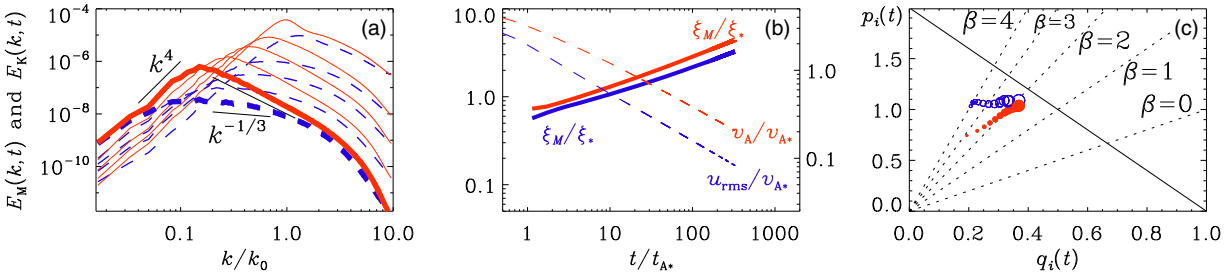

FIG. 1. Run A with $Q_\star = 10$, $\mathrm{Re} = 130$, Batchelor spectrum $\alpha = 4$, so $\nu_\star = 10^{-5}c_{\mathrm{s}}/k_1$ and $r = -0.43$ are used, and no helicity is applied, i.e., $\sigma_{\mathrm{M}} = \sigma_{\mathrm{K}} = 0$. (a) E_{M} (red, solid) and E_{K} (blue, dashed) at times $t/t_{\mathrm{A}\star} = 4$, 30, 120, 500, and 2000. The last time is indicated by thick lines. (b) $\xi_{\mathrm{M}}/\xi_\star$ (red, thick) and $\xi_{\mathrm{K}}/\xi_\star$ (blue, thick) with scale on the left, together with $v_{\mathrm{A}}/v_{\mathrm{A}\star}$ (red, dashed) and $u_{\mathrm{rms}}/v_{\mathrm{A}\star}$ (blue, dashed) with scale on the right. (c) pq diagram showing the evolution of $\boldsymbol{P}_{\mathrm{M}}$ (red, filled symbols) and $\boldsymbol{P}_{\mathrm{K}}$ (blue, open symbols). The symbol size increases with time. The equilibrium line $p = 2(1 - q)$ is shown as solid, while the $\beta = \mathrm{const}$ lines are dotted.

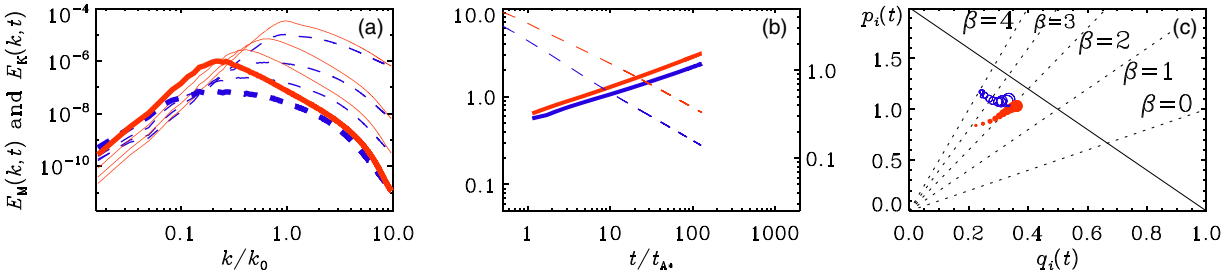

FIG. 2. Same as Fig. 1, but for Run B with $Q_\star = 1$ and $\mathrm{Re} = 100$. The times in (a) are $t/t_{\mathrm{A}\star} = 4$, 40, 180, and 800.

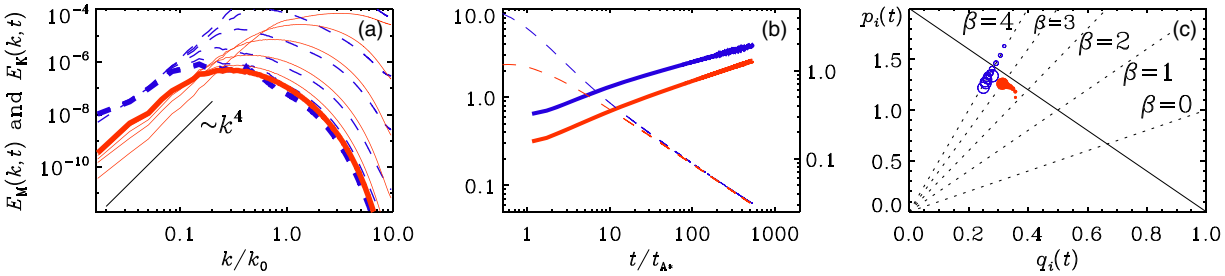

FIG. 3. Same as Fig. 1, but for Run C with $Q_\star = 0.1$ and Re = 35. The times in (a) are $t/t_{A\star} = 0.4$, 4, 18, 80, and 200.

out to be close to 1 instead of the present value of 2. For Run C, on the other hand, even though Q was initially 0.1, it reaches unity at later times; see Fig. 3.

Indeed, comparing the pq diagrams for all three cases, we see again that for Runs A and B, both $\boldsymbol{P}_M$ and $\boldsymbol{P}_K$ evolve along the $\beta = 2$ line toward the equilibrium line where $p = 2(1-q)$ and thus $p = 6/5$ and $q = 2/5$. By contrast, for Run C, the $\boldsymbol{P}_i$ (with $i = M$ and K) evolve towards the $\beta = 4$ line. Furthermore, the $\boldsymbol{P}_i$ seem to move away from the equilibrium line. At present, we do not know whether this could be an artifact of limited scale separation (k/k_1 is too small) for small values of k and also of the limited inertial range between k_0 and the dissipation wave number above which the spectra stop being power laws.

B. White-noise spectrum and no helicity

Let us now turn to simulations with $\alpha = 2$, which was recently studied in Ref. [8], where it was found that no inverse transfer occurs in that case. Here we also compare with simulations where an additional Gaussian profile is included in the initial spectrum ($\mathcal{G} = 1$); see Eq. (24). We only consider cases where $Q_\star = 1$ or $\to \infty$.

TABLE I. Summary of our runs.

Run	σ_K	σ_M	α	$\mathcal{G}$	$Q_\star$	Q_e	$t_e/t_{A\star}$	β_M	q_M	p_M	Figure[a]
BKT	0	0	4	0	∞	2.8	1335	1.2	0.47	1.02	Ref. [58]
A	0	0	4	0	10	2.5	206	1.8	0.37	1.04	Fig. 1
B	0	0	4	0	1	2.4	114	1.9	0.36	1.03	Fig. 2
C	0	0	4	0	0.1	1.0	460	3.0	0.31	1.26	Fig. 3
D	0	0	2	0	1	3.2	208	1.7	0.38	1.03	Fig. 4
E	0	0	2	1	1	2.6	170	1.7	0.36	0.95	Fig. 5
F	0	0	2	1	∞	2.6	170	1.7	0.35	0.94	Fig. 6
G	0	0.03	2	1	1	3.2	1024	0.3	0.55	0.73	Fig. 7
H	1	1	4	0	1	1.3	562	0.6	0.46	0.76	Fig. 8
I	1	0	4	0	1	2.3	1250	0.2	0.49	0.58	Fig. 9
J	1	−1	4	0	1	2.9	460	0.1	0.48	0.57	Fig. 10
BK	0	1	4	0	∞	4.2	1025	0.0	0.59	0.62	Ref. [55]

[a]BKT refers to the nonhelical run of Ref. [58] and BK to a fully helical of Ref. [55]. $Q_\star$ and Q_e refer to the values of Q at the beginning and end of the run, respectively. The instantaneous scaling exponents β_M, q_M, and p_M are given at the end of the run, whose normalized end time $t_e/t_{A\star}$ is given.

Not surprisingly, the cases with $\mathcal{G} = 0$ (Run D; see Fig. 4) and $\mathcal{G} = 1$ (Run D; see Fig. 5) are rather similar, except that the early time evolution is closer to equipartition We also compare with the case $Q_\star \to \infty$ (Run F). Again, it has the same late-time evolution as Runs D and E, but the early time evolution is now close to that of Run D; see Fig. 6.

In all these cases, $\boldsymbol{P}$ evolves along the $\beta = 2$ line towards the equilibrium line. This implies that in these cases there is no inverse transfer; see Eq. (33). This is consistent with Ref. [8]. As we already noted, the white noise spectrum for the initial magnetic field has only academic interest because we expect causality to limit the power on large length scales to subwhite noise levels; see footnote 2.

C. White-noise spectrum with magnetic helicity

The case of fractional helicity has been studied previously [12] in connection with QCD phase transition-created initial magnetic fields. In these studies, $\alpha = 4$ was used, but the resolution was only 512^3.

We now discuss the case with $\alpha = 2$ (Run G). In contrast to the earlier case with $\alpha = 4$ [12], there is now no inverse transfer at early times when the magnetic energy is still strong. As in earlier work, we plot the evolution of ξ_M, as defined in Eq. (14), which increases like $t^{1/2}$. We compare this with $\xi_M^{\rm min}$, defined in Eq. (17), which increases with time since $\mathcal{H}_M(t) = \text{const}$ and $\mathcal{E}_M \propto t^{-1}$. The result is shown in Fig. 7. Evidently, $\xi_M^{\rm min}(t) \propto t$, and so $\xi_M^{\rm min}(t)$ will be equal to ξ_M after some time. The initial value of $\xi_M^{\rm min}(t)$ depends on the fractional helicity and is given by $\epsilon_M k_0^{-1}$. It turns out that the late-time subinertial spectrum for the magnetic field changes from a k^2 (white noise spectrum) to a k^4 (Batchelor spectrum) at the time when the magnetic field begins to be fully helical. This change of slope was also found for $\sigma_M = 0.1$ [55].

D. Batchelor spectrum with initial kinetic helicity

The initial presence of kinetic helicity has profound effects on the evolution of the magnetic field. Kinetic helicity leads to an α effect, i.e., the destabilization of a large-scale magnetic field. The details of this process in decaying turbulence were studied in Ref. [37], where it was

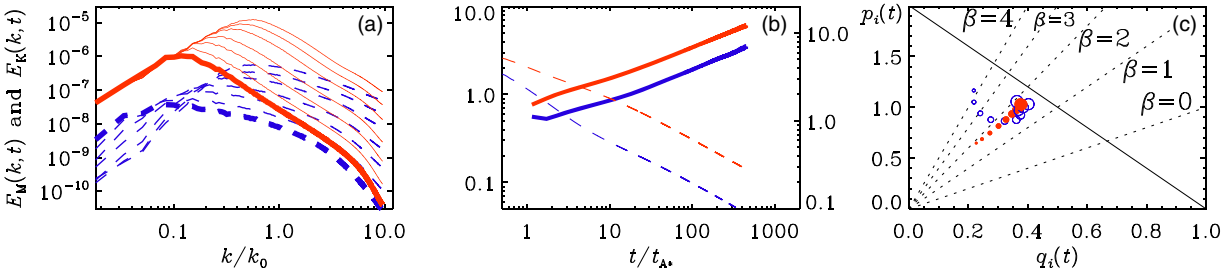

FIG. 4. Similar to Fig. 1, but for Run D with $Q_\star = 1$, Re $= 600$, and $\alpha = 2$, so $\nu_\star = 10^{-6} c_s/k_1$ and $r = -0.20$ are used. The times in (a) are $t/t_{A\star} = 40$, 80, 150, 400, 800, 1600, and 3000.

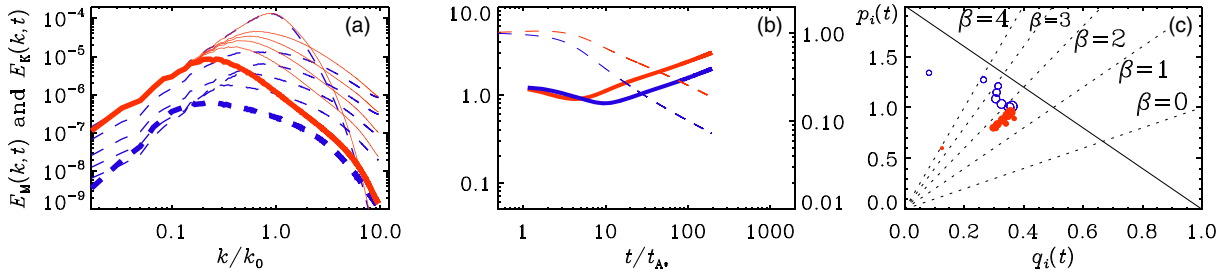

FIG. 5. Same as Fig. 4, but for Run E with $\mathcal{G} = 1$ and Re $= 200$. The times in (a) are $t/t_{A\star} = 0.6$, 6, 12, 20, 50, and 200.

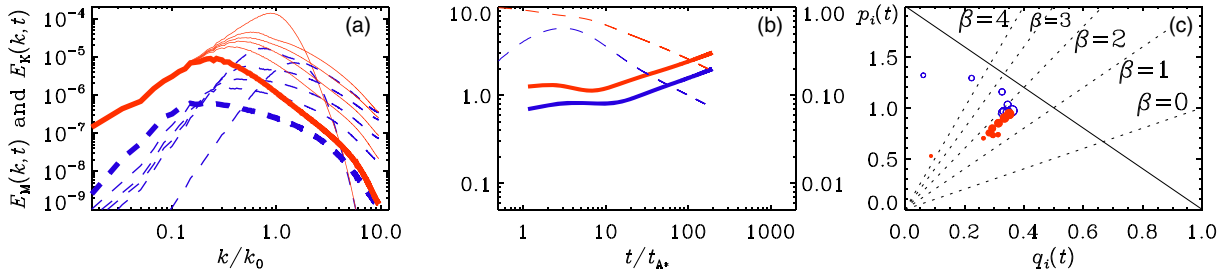

FIG. 6. Same as Fig. 5, but for Run F with $Q_\star \to \infty$, i.e., $u_\star = 0$, and Re $= 200$. The times in (a) are $t/t_{A\star} = 0.6$, 6, 12, 20, 50, and 200.

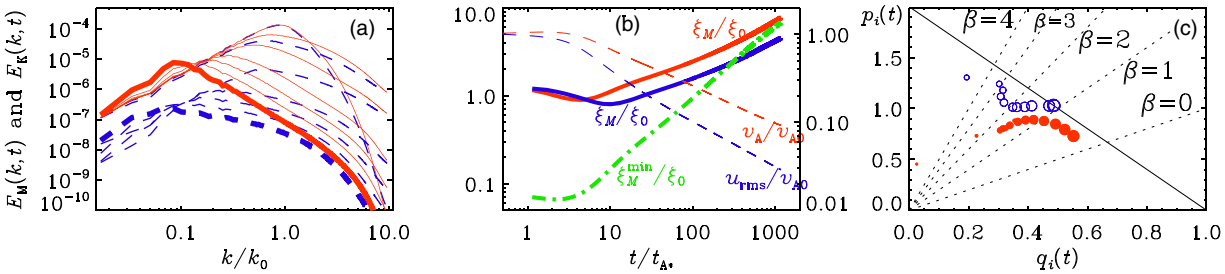

FIG. 7. Similar to Fig. 5, but for Run G with $\sigma_M = 0.03$ and Re $= 300$. The times in (a) are $t/t_{A\star} = 0.6$, 4, 18, 120, 300, 600, and 1200. In (b), the evolution of $\xi_M^{\rm min}$ is shown as a green dashed-dotted line.

found that the initial kinetic helicity gets transformed efficiently into magnetic helicity such that the residual helicity, $\langle \boldsymbol{\omega} \cdot \boldsymbol{u} \rangle - \langle \boldsymbol{J} \cdot \boldsymbol{B} \rangle / \rho_\star$ is approximately constant. During the time of their runs, the magnetic helicity $\langle \boldsymbol{A} \cdot \boldsymbol{B} \rangle$ was still increasing, so one expects to reach the familiar behavior with $p_i = q_i = 2/3$ at much later times.

In Table I, the corresponding results for p and q from Ref. [55] are marked with BK. $\boldsymbol{P}_i$ evolves towards

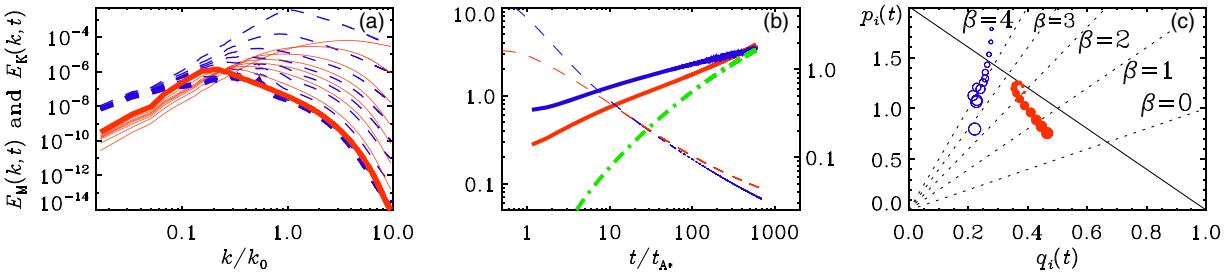

FIG. 8. Similar to Fig. 2, but for Run H with $\sigma_K = \sigma_M = 1$ and Re $= 65$. The times in (a) are $t/t_A = 0.5$, 3, 10, 25, 50, 100, 250, and 500.

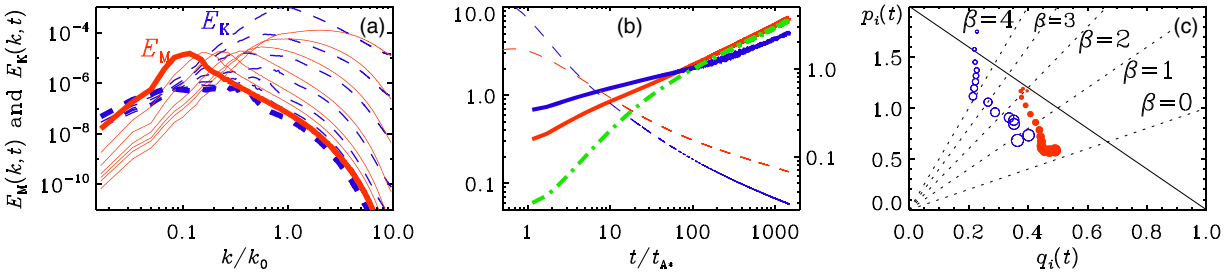

FIG. 9. Similar to Fig. 8, but for Run I with $\sigma_K = 1$, $\sigma_M = 0$ and Re $= 160$. The times in (a) are $t/t_A = 1$, 4, 14, 60, 180, and 600.

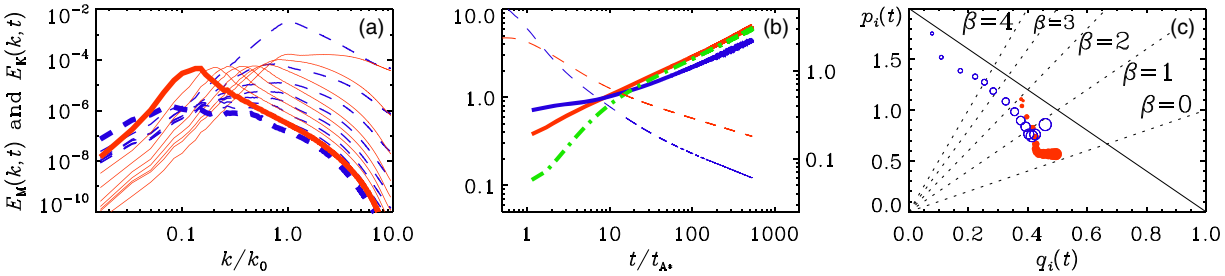

FIG. 10. Similar to Fig. 8, but for Run J with $\sigma_K = 1$, $\sigma_M = -1$ and Re $= 160$. The times in (a) are $t/t_A = 0.5$, 3, 10, 25, 50, 100, 250, and 500.

the $\beta = 0$ line, but it is still far away from the ultimate equilibrium line $p = 2(1-q)$. Instead, we see that in Figs. 8–10, $q_M = 0.4$–0.5 during an extended time interval, and that $p_M = 0.5$–0.6, while in the equilibrium state we would expect $p_M = 1.2$–1.0.

E. Comparison with the equilibrium line

In Table II, we summarize the anticipated values of q and p that would be expected for given values of q or β if the solutions were to lie on the equilibrium line in the pq diagram. These different cases are based on the dimensions of potentially conserved quantities such as the Loitsiansky and Saffman integrals,

$$\mathcal{L} = \int \boldsymbol{r}^2 \langle \boldsymbol{u}(\boldsymbol{x}) \cdot \boldsymbol{u}(\boldsymbol{x}+\boldsymbol{r}) \rangle d\boldsymbol{r} \propto \ell^5 u_\ell^2 \tag{34}$$

and

$$\mathcal{S} = \int \langle \boldsymbol{u}(\boldsymbol{x}) \cdot \boldsymbol{u}(\boldsymbol{x}+\boldsymbol{r}) \rangle d\boldsymbol{r} \propto \ell^3 u_\ell^2, \tag{35}$$

respectively [59], with typical velocity u_ℓ on scale ℓ, the conservation of magnetic helicity, $\langle \boldsymbol{A} \cdot \boldsymbol{B} \rangle$, and the possible

TABLE II. Scaling exponents and relation to physical invariants and their dimensions.

β	q	p	inv.	dim.
4	$2/7 \approx 0.286$	$10/7 \approx 1.43$	$\mathcal{L}$	$[x]^7[t]^{-2}$
2	$2/5 = 0.400$	$6/5 = 1.20$	$\mathcal{S}$	$[x]^5[t]^{-2}$
1	$2/4 = 0.500$	$4/4 = 1.00$	$\langle \boldsymbol{A}_{2D}^2 \rangle$	$[x]^4[t]^{-2}$
0	$2/3 \approx 0.667$	$2/3 \approx 0.67$	$\langle \boldsymbol{A} \cdot \boldsymbol{B} \rangle$	$[x]^3[t]^{-2}$

conservation of the mean squared vector potential, $\langle \boldsymbol{A}^2 \rangle$, which is known to be conserved in two dimensions (2D).

Comparing with the numerical results given in Table I, we see that for the runs with fractional magnetic helicity or with initial kinetic helicity, there is a tendency to develop maximal magnetic helicity at later times. As a consequence, all those runs are seen to develop toward the $\beta = 0$ line. However, in none of those runs there is a perfect convergence toward the equilibrium point with $p = q = 2/3$, as would be expected in the fully helical case. Instead, we find that $q \approx 0.5$ and $p \approx 0.6$, so the decay is even slower than with maximum helicity.

The departure from the expected equilibrium position may well be a finite size effect of the computational domain. Ideally, one would like to have a much larger numerical resolution, so as to be able to follow an unimpeded development of the inverse cascade for both $E_{\rm M}$ and $E_{\rm K}$ toward smaller wave numbers. At the same time, of course, it is important to include large enough wave numbers to resolve the turbulent inertial and dissipative subranges.

In most of the runs without kinetic or magnetic helicity, the final values of q are in the range 0.3–0.4, which is again smaller than what is expected for the equilibrium points $(p, q) = (0.5, 1)$, when $\beta = 1$ or (0.4, 1.2), when $\beta = 2$; see Table II. In those cases, on the other hand, there is a clear trend that (p, q) evolves along the $\beta = 2$ line towards the equilibrium point; see Figs. 1 and 2 for $\alpha = 4$ and Figs. 4–6 for $\alpha = 2$.

Interestingly, the two groups of runs for $\alpha = 4$ and $\alpha = 2$ show the same convergence properties along the $\beta = 2$ line toward the equilibrium point $(p, q) = (0.4, 1.2)$. This decay law is suggestive of the case where the Saffman integral (35) is conserved. Thus, what we have here is a clear example where the temporal evolutions of $\mathcal{E}_{\rm M}$ and $\xi_{\rm M}$ are independent of the initial slope α: the case with $\alpha = 4$ shows inverse cascading while that with $\alpha = 2$ does not, as expected based on Eq. (33).

The subequipartition case with $Q_\star = 0.1$ is different again; see Fig. 3, where we observe a clear development along the $\beta = 4$ line toward the equilibrium point on which the Loitsiansky integral (34) is expected to be conserved.

V. DISCUSSION

This work has exposed several unknown behaviors of decaying MHD turbulence. First, for nonhelical turbulence with an $\alpha = 4$ Batchelor spectrum, large initial values of $Q_\star$ (here $Q_\star = 1$ and 10) lead to distinctly different behaviors than small values (here $Q_\star = 0.1$). While the former case yields $Q_{\rm e} \equiv Q(t_{\rm e}) \approx 3$ at the end of our runs (at $t = t_{\rm e}$), the latter case yields $Q(t_{\rm e}) \approx 1$; see Run C in Table I. There is at present no indication that all these cases yield ultimately the same late-time behavior. However, we cannot exclude the possibility that large and small initial $Q_\star$ values yield ultimately the same final $Q_{\rm e}$ value.

Second, in the case with $\alpha = 2$, no inverse transfer was found to be possible. This is because that case also yields $\beta = 2$, and so $\alpha = \beta$, which implies that no inverse transfer is possible; see Eq. (33). This is compatible with recent work by Reppin and Banerjee [8].

Third, in the case with initial kinetic helicity, a non scale-invariant behavior is found during an extended period of time where the points $\boldsymbol{P}_{\rm K}$ and $\boldsymbol{P}_{\rm M}$ evolve away from the equilibrium line, $p = 2(1 - q)$.

In view of the early Universe, an important lesson is the fact that even just a small amount of magnetic or kinetic helicity yields the standard fully helical inverse transfer after a certain time. The situation is similar in the case where there is only kinetic helicity initially. In both cases, $\beta_{\rm M} \approx 0$, which implies that $p_{\rm M} = q_{\rm M}$; see Eq. (29). This also means that $B_{\rm rms} \propto \xi_{\rm M}^{-1/2}$. However, unlike the case with initial magnetic helicity where $p_{\rm M} = q_{\rm M} = 2/3$, we find here $p_{\rm M} \approx q_{\rm M} \approx 1/2$ during an extended period of time; see Figs. 9 and 10. Ultimately, at very late times, we might still expect $p_{\rm M} = q_{\rm M} = 2/3$, but the time required for this to happen may be too long.

To put our results into perspective, it is instructive to consider the evolution of $B_{\rm rms}$ as a function of $\xi_{\rm M}$, which, in turn, is a function of time and thus of the scale factor or the inverse temperature of the Universe. The turbulent evolution of $B_{\rm rms}$ and $\xi_{\rm M}$ proceeds from the time of magnetic field generation until recombination. This implies an increase in the conformal time by twelve orders of magnitude, and thus eight orders of magnitude in $\xi_{\rm M} \propto t^{2/3}$, if the initial magnetic field is fully helical. On the other hand, if there is only initial kinetic helicity, and if the $\xi_{\rm M} \propto t^{1/2}$ decay law persists for a significant fraction of time, we might only cover about six orders of magnitude in $\xi_{\rm M}$, but the field will not decay by as much as in the former case.

Turning now to the cosmological applications of our results, we are interested in predicting the magnetic field characteristics at the epoch of recombination, $t_{\rm rec}$, for initial conditions specified at some earlier epoch, $t_\star$. In Appendix B we show that, if there is sufficient time for the magnetic field to reach maximal helicity, and if it is not caused by initial kinetic helicity (which leads to $p \approx q \approx 0.5$ for a long period of time, as in Run I), then

$$\frac{B_{\rm rec}}{\xi_{\rm rec}} = \frac{B_\star}{\xi_\star} \left(\frac{t_{\rm rec}}{t_\star} \right)^{-1}. \tag{36}$$

This result is independent of the initial hydromagnetic state and provides a universal result, applicable to a large number of cases we have considered. Note that $t_\star / t_{\rm rec} = T_{\rm rec} / T_\star$.

Let us now discuss the different turbulent decay scenarios for two cases, the best case scenario where a magnetic field is generated at the horizon scale with a strength limited by BBN and the second case where magnetic helicity is generated by the chiral magnetic effect; see Fig. 11. In the former case, if the initial field is fully helical, we will reach a magnetic field at a scale of 30 kpc with a strength of 0.3 nG. If we only have kinetic helicity initially, and if the

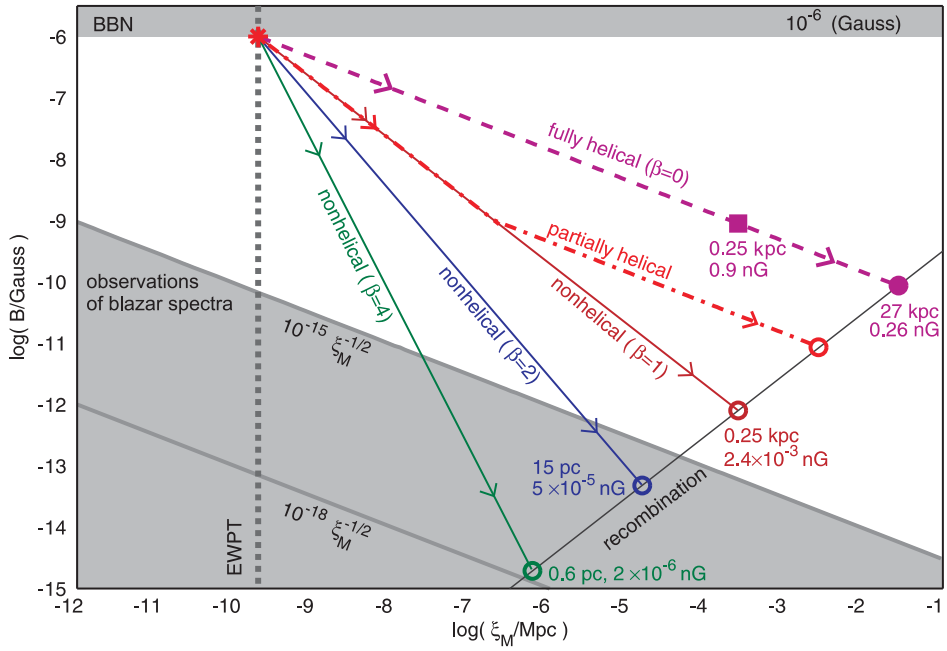

FIG. 11. Turbulent evolution of $B_{\rm rms}$ and $\xi_{\rm M}$ starting from their upper limits given by the BBN bound and the horizon scale at the electroweak phase transition (EWPT) for the fully helical case ($B_{\rm rms} \propto \xi_{\rm M}^{-1/2}$), the nonhelical case ($B_{\rm rms} \propto \xi_{\rm M}^{-1}$), and the fractionally helical case with $\epsilon_{\rm M\star} = 10^{-3}$. Circles indicate the final points at recombination for zero or partial initial magnetic helicity, the filled circle marks the fully helical case, and the filled square indicates the case with initial kinetic helicity. The regimes excluded by observations of blazar spectra are marked in gray. The upper boundary of the gray area corresponds to the lower bound claimed in [62] based on the deficit of blazar gamma rays in the GeV band as compared to the flux expected due to the inverse cascade while assuming that the mean blazar TeV flux remains constant. The bottom line in the gray area shows the lower bounds while assuming that the TeV flux activity is limited by the source observation period (few years) [60,61]. The end of the evolution at recombination is denoted by the straight line given by the relation in Eq. (36), and the final values of $B_{\rm rms}$ and $\xi_{\rm M}$ are indicated for helical and nonhelical scenarios.

$\xi_{\rm M} \propto t^{1/2}$ behavior persists during the whole time, we might even get 3 nG, but only on a scale of 0.3 kpc. If the magnetic field stays nonhelical during the entire time, and if turbulence is magnetically dominated, the field would again be of a typical scale of about 0.3 kpc, but now the field is significantly weaker—about 3×10^{-3} nG. Even magnetic fields amplified by the chiral magnetic effect cannot have helicity in excess of $\langle \boldsymbol{B}^2 \rangle \xi_{\rm M} \approx 5 \times 10^{-38} {\rm G}^2\,{\rm Mpc}$ if the chiral asymmetry is set by the temperature [33]. This might still be compatible with the most conservative lower limits on the magnetic field strength derived from blazar spectra, when accounting for the fact that the TeV flux activity is limited by the source observation period (few years) [60,61], but not with stronger fields on large length scales claimed in Ref. [62] through the assumption of a constant mean blazar TeV flux.

VI. CONCLUSIONS

To understand the evolution of cosmic magnetic fields, we have considered a broad range of different initial conditions: magnetically and kinetically dominated cases, with and without helicity either in the magnetic or the velocity field, as well as with shallow and steeper initial energy spectra. Our results are best summarized by presenting them parametrically in the $B_{\rm rms}$ versus $\xi_{\rm M}$ diagram discussed in Sec. V. The resulting trajectories have different slopes, $-(1+\beta)/2$, and cover different extents in $\Delta \log \xi_{\rm M} = q \Delta \log t$ in time. The most shallow slope is $1/2$ in the helical case, where $\beta = 0$. This is independent of whether helicity is initially in the magnetic field or in the velocity.

Although the two cases are essentially the same as far as the slope is concerned, there is a difference in terms of the length scales covered during the evolution. The largest range of scales is covered when the initial magnetic field is fully helical and $q = 2/3$, but is $q = 1/2$ when only the velocity is initially helical. Consequently, because $p = q$ in the fully helical case, the magnetic field decays less in the latter case. However, it is not clear whether there is any physical mechanism that can create kinetic helicity throughout the entire Universe. Familiar effects in dynamo theory that involve rotation and nonuniformity always produce positive and negative signs at the same time, so there is no net effect on larger scales. For the magnetic field, on the other hand, this limitation does not apply if it is created through non-MHD effects such as the chiral magnetic effect. One exception is the chiral vortical effect

[32], but since the chiral asymmetry is expected to be set by the temperature, chiral effects will be constrained as explained in Eq. (2) of the Introduction. This now seems to be excluded by the observations of blazar spectra, which are in agreement with the conclusions of Ref. [7].

ACKNOWLEDGMENTS

It is our pleasure to thank Andrey Beresnyak, Alexey Boyarsky, Ruth Durrer, Arthur Kosowsky, Andrii Neronov, and Oleg Ruchayskiy for useful discussions. We thank NORDITA for hospitality and support during the course of this work. T. K. also thanks the High Energy and Cosmology division and the Associate Membership Program at International Center for Theoretical Physics (ICTP) for hospitality and partial support. T. V. also thanks Institute for Advanced Study, Princeton, for hospitality while this work was being completed. Support through the NSF Astrophysics and Astronomy Grant (AAG) Program (Grants No. AST1615940 and No. AST1615100), the Research Council of Norway (FRINATEK Grant No. 231444), the Swiss NSF SCOPES (Grant No. IZ7370-152581), and the Georgian Shota Rustaveli NSF (Grant No. FR/264/6-350/14) are gratefully acknowledged. T. V. is supported by the U.S. Department of Energy Award No. DE-SC0018330 at ASU. We acknowledge the allocation of computing resources provided by the Swedish National Allocations Committee at the Center for Parallel Computers at the Royal Institute of Technology in Stockholm. This work utilized the Janus supercomputer, which is supported by the National Science Foundation (Award No. CNS-0821794), the University of Colorado Boulder, the University of Colorado Denver, and the National Center for Atmospheric Research. The Janus supercomputer is operated by the University of Colorado Boulder.

APPENDIX A: COMPARISON WITH THE STANDARD MHD EQUATIONS

The purpose of this appendix is to contrast Eqs (19)–(21) with the usual MHD equations for an isothermal gas, i.e.,

$$\frac{\partial \ln\rho}{\partial t} = -(\boldsymbol{\nabla}\cdot\boldsymbol{u} + \boldsymbol{u}\cdot\boldsymbol{\nabla}\ln\rho), \tag{A1}$$

$$\frac{\mathrm{D}\boldsymbol{u}}{\mathrm{D}t} = -\frac{1}{3}\boldsymbol{\nabla}\ln\rho + \frac{1}{\rho}\boldsymbol{J}\times\boldsymbol{B} + \frac{2}{\rho}\boldsymbol{\nabla}\cdot(\rho\nu\mathsf{S}), \tag{A2}$$

$$\frac{\partial \boldsymbol{B}}{\partial t} = \nabla\times(\boldsymbol{u}\times\boldsymbol{B} - \eta\boldsymbol{J}). \tag{A3}$$

In Fig. 12 we show a comparison of magnetic and kinetic energy spectra for a low resolution version of Run I for the relativistic and nonrelativistic equation of state. (This run is identical to Run A of Ref. [37].) Note that the magnetic energy spectra are virtually the same, but the kinetic energy is slightly (factor $4/3$) less in the relativistic case where $Q_\star = 1$; see panel (a). For the case where $Q_\star = 0.1$, the magnetic energy is slightly (factor $4/3$) larger; see panel (b).

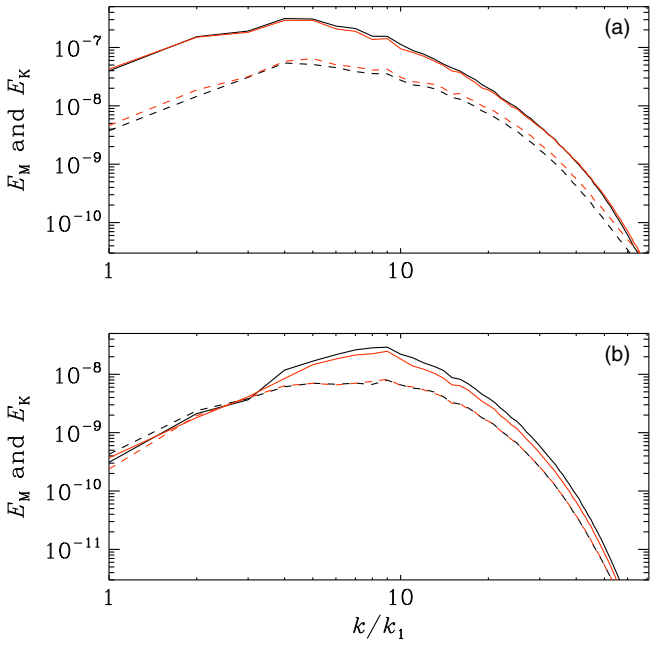

FIG. 12. Magnetic energy spectra (solid lines) and kinetic energy spectra (dashed lines) for decaying MHD turbulence. Black (red) lines are for the relativistic (nonrelativistic) equation of state with (a) $Q_\star = 1$ and (b) $Q_\star = 0.1$.

APPENDIX B: THE RESULTING MAGNETIC FIELD CHARACTERISTICS

Accounting for the scaling laws obtained for the runs summarized in Table I, the (comoving) correlation length and the mean (comoving) magnetic energy density at time t for the ith run are given as

$$\xi^{(i)} = \xi_\star^{(i)}\left(\frac{t}{t_\star}\right)^{q_i}, \qquad \mathcal{E}_{\rm M}^{(i)} = \mathcal{E}_{\rm M\star}^{(i)}\left(\frac{t}{t_\star}\right)^{-p_i}. \tag{B1}$$

Correspondingly, the magnetic field rms amplitude is

$$B_{\rm rms}^{(i)} = B_{\star,\rm rms}^{(i)}\left(\frac{t}{t_\star}\right)^{-p_i/2}. \tag{B2}$$

Let us consider MHD turbulence decay laws that conserve different invariants during the turbulent decay process. In this case the scaling exponents can be calculated using Table II, where $\beta = p/q - 1$ can be used as subscript instead of the "i". Hence we use p_β and q_β with $\beta = 1, 2, 4$ for nonhelical and partially helical fields and $p_0 = q_0 = 2/3$ for the case of fully helical decay.

If the initial magnetic fields are only partially helical, the first evolutionary stage consists of the field developing

towards maximal helicity. During this period, the growth of the correlation length is slower: $\sim t^{1/2}$ for nonhelical compared to $\sim t^{2/3}$ for fully helical cases in the magnetically dominant scenarios. Also, in this period the mean magnetic energy density decay is faster: $\sim t^{-1}$ for nonhelical compared to $\sim t^{-2/3}$ for fully helical cases in the magnetically dominant scenarios. The fractional helicity grows during the turbulence decay process and reaches a state with maximal helicity at the time [12]

$$t_{\rm hel} = t_\star (\epsilon_{{\rm M},\star})^{-1/q_\beta}, \tag{B3}$$

where $\epsilon_{{\rm M}\star} = \epsilon_{\rm M}(t_\star)$ and $\epsilon_{\rm M}$ is defined in Eq. (23).

The generation of the magnetic (and/or velocity) field occurs deep in the radiation dominated epoch during which $a \propto t$ (i.e., the conformal time) while the ending evolution proceeds during the matter dominated epoch when $a \propto t^2$. To compute the magnetic field characteristics at recombination $t_{\rm rec}$, namely the rms magnetic field amplitude $B_{\rm rec}$ and the correlation length $\xi_{\rm rec}$, we first calculate the correlation length and the rms magnetic field when the fully helical state is reached:

$$\xi_{\rm hel} = \xi_\star \left(\frac{t_{\rm hel}}{t_\star}\right)^{q_\beta}, \qquad B_{\rm hel} = B_\star \left(\frac{t_{\rm hel}}{t_\star}\right)^{-p_\beta/2}, \tag{B4}$$

where q_β (p_β) is the correlation length scale growth (the mean magnetic energy density decay) index during the first partially helical stage: $\beta = 1, 2, 4$. If the fully helical stage is reached before recombination, the correlation length and the rms magnetic field at recombination can be calculated as follows:

$$\xi_{\rm rec} = \xi_{\rm hel} \left(\frac{t_{\rm rec}}{t_{\rm hel}}\right)^{q_0}, \qquad B_{\rm rec} = B_{\rm hel} \left(\frac{t_{\rm rec}}{t_{\rm hel}}\right)^{-p_0/2}, \tag{B5}$$

with q_0 (p_0) referring to the correlation length (the mean magnetic energy) growth (decay) index during the second helical stage. It is easy to see that

$$\begin{aligned} \xi_{\rm rec} &= \xi_\star \left(\frac{t_{\rm rec}}{t_\star}\right)^{q_0} (\epsilon_{{\rm M}\star})^{-(q_\beta - q_0)/q_\beta}, \\ B_{\rm rec} &= B_\star \left(\frac{t_{\rm rec}}{t_\star}\right)^{-p_0/2} (\epsilon_{{\rm M}\star})^{(p_\beta - p_0)/2q_\beta}. \end{aligned} \tag{B6}$$

Recalling the definition of the β parameter and the pq equilibrium condition (see Sec. III C), we can express the scaling exponents as follows:

$$q_\beta = \frac{2}{\beta+3}, \qquad p_\beta = \frac{2}{\beta+3}(\beta+1). \tag{B7}$$

Hence Eqs. (B6) and (B7) show that the ratio of the correlation length and the mean magnetic field amplitude at recombination does not depend on the (fractional) helicity of the initial magnetic field[8] $\epsilon_{{\rm M}\star}$ or the β parameter itself:

$$\frac{B_{\rm rec}}{\xi_{\rm rec}} = \frac{B_\star}{\xi_\star}\left(\frac{t_{\rm rec}}{t_\star}\right)^{-1}. \tag{B8}$$

This helps to set a common recombination limit for different types of turbulent decay. On the other hand, the mean magnetic field amplitude and the corresponding correlation length of nonhelical or weakly helical fields, when there is not sufficient time to reach a fully helical state before recombination, can be calculated as:

$$B_{\rm rms} = B_\star \left(\frac{\xi_{\rm M}}{\xi_\star}\right)^{-(\beta+1)/2}. \tag{B9}$$

Figure 11 shows the evolution of the mean turbulent magnetic field amplitude with respect to the correlation length $\xi_{\rm M}$ for different classes of MHD turbulence. Initial values ($\xi_\star$, $B_\star$) correspond to the maximal values set by BBN constraints at the electroweak epoch.

We provide some numerical estimates of the growth of correlation lengths for the magnetically dominant case. We take $\xi_{{\rm M},\star}$ to be the maximum comoving Hubble radius at the epoch of electroweak phase transition, given by (9), and note that at recombination, the temperature was $\sim$0.25 eV. The correlation length evolution relations stated above can be plotted as in Fig. 13.

We have used the fact that the conformal time is expressed in terms of the scale factor $a_{\rm eq}$ at the epoch of matter-radiation equality and the fractional matter density $\Omega_{m,0}$ as

$$t(a) = \frac{2}{\sqrt{\Omega_{m,0}} H_0}\left[\sqrt{a_{\rm eq}+a} - \sqrt{a_{\rm eq}}\right], \tag{B10}$$

and that the effective degrees of freedom of the particle species are roughly constant throughout.

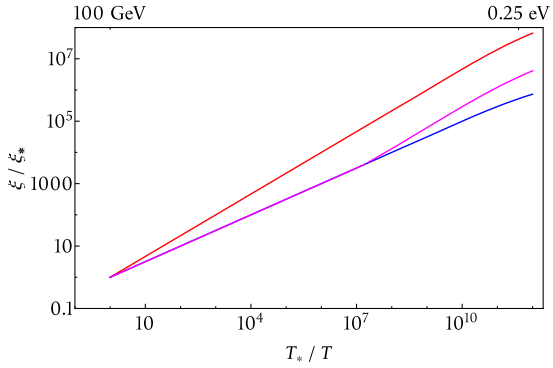

FIG. 13. Ratio of correlation lengths, $\xi_{\rm M}/\xi_{{\rm M}\star}$, for magnetically dominant cases for nonhelical (blue), fully helical (red), and fractionally helical ($\sigma_\star = 0.03$; magenta) cases.

[8]Note that in the case of initial kinetic helicity (which leads to $p \approx q \approx 0.5$; see the square in the Fig. 11), $B_{\rm rec}/\xi_{\rm rec}$ does depend on the initial magnetic helicity $\epsilon_{\rm M}$.

[1] L. M. Widrow, Rev. Mod. Phys. **74**, 775 (2002).
[2] R. M. Kulsrud and E. G. Zweibel, Rep. Prog. Phys. **71**, 046901 (2008).
[3] A. Kandus, K. E. Kunze, and C. G. Tsagas, Phys. Rep. **505**, 1 (2011).
[4] R. Durrer and A. Neronov, Astron. Astrophys. Rev. **21**, 62 (2013).
[5] C. J. Hogan, Phys. Rev. Lett. **51**, 1488 (1983).
[6] T. Kahniashvili, A. G. Tevzadze, A. Brandenburg, and A. Neronov, Phys. Rev. D **87**, 083007 (2013).
[7] J. M. Wagstaff and R. Banerjee, J. Cosmol. Astropart. Phys. 01 (2016) 002.
[8] J. Reppin and R. Banerjee, Phys. Rev. E **96**, 053105 (2017).
[9] R. Banerjee and K. Jedamzik, Phys. Rev. D **70**, 123003 (2004).
[10] A. Brandenburg and K. Subramanian, Phys. Rep. **417**, 1 (2005).
[11] T. A. Ensslin, Astron. Astrophys. **401**, 499 (2003).
[12] A. G. Tevzadze, L. Kisslinger, A. Brandenburg, and T. Kahniashvili, Astrophys. J. **759**, 54 (2012).
[13] A. J. Long, E. Sabancilar, and T. Vachaspati, J. Cosmol. Astropart. Phys. 02 (2014) 036.
[14] T. Fujita and K. Kamada, Phys. Rev. D **93**, 083520 (2016).
[15] K. Kamada and A. J. Long, Phys. Rev. D **94**, 063501 (2016).
[16] K. Kamada and A. J. Long, Phys. Rev. D **94**, 123509 (2016).
[17] T. Vachaspati, Phys. Lett. B **265**, 258 (1991).
[18] J. M. Cornwall, Phys. Rev. D **56**, 6146 (1997).
[19] M. Giovannini and M. E. Shaposhnikov, Phys. Rev. D **57**, 2186 (1998).
[20] M. Joyce and M. E. Shaposhnikov, Phys. Rev. Lett. **79**, 1193 (1997).
[21] G. B. Field and S. M. Carroll, Phys. Rev. D **62**, 103008 (2000).
[22] M. M. Forbes and A. R. Zhitnitsky, Phys. Rev. Lett. **85**, 5268 (2000).
[23] T. Vachaspati, Phys. Rev. Lett. **87**, 251302 (2001).
[24] G. Sigl, Phys. Rev. D **66**, 123002 (2002).
[25] K. Subramanian and A. Brandenburg, Phys. Rev. Lett. **93**, 205001 (2004).
[26] A. Diaz-Gil, J. Garcia-Bellido, M. Garcia Perez, and A. Gonzalez-Arroyo, Phys. Rev. Lett. **100**, 241301 (2008).
[27] T. Stevens, M. B. Johnson, L. S. Kisslinger, E. M. Henley, W.-Y. P. Hwang, and M. Burkardt, Phys. Rev. D **77**, 023501 (2008).
[28] C. J. Copi, F. Ferrer, T. Vachaspati, and A. Achucarro, Phys. Rev. Lett. **101**, 171302 (2008).
[29] Y. Ng and T. Vachaspati, Phys. Rev. D **82**, 023008 (2010).
[30] Y. Z. Chu, J. B. Dent, and T. Vachaspati, Phys. Rev. D **83**, 123530 (2011).
[31] A. Boyarsky, J. Fröhlich, and O. Ruchayskiy, Phys. Rev. Lett. **108**, 031301 (2012).
[32] H. Tashiro, T. Vachaspati, and A. Vilenkin, Phys. Rev. D **86**, 105033 (2012).
[33] A. Brandenburg, J. Schober, I. Rogachevskii, T. Kahniashvili, A. Boyarsky, J. Fröhlich, O. Ruchayskiy, and N. Kleeorin, Astrophys. J. **845**, L21 (2017).
[34] T. Vachaspati, Phys. Rev. D **95**, 063505 (2017).
[35] A. Nicolis, Classical Quantum Gravity **21**, L27 (2004).
[36] M. Christensson, M. Hindmarsh, and A. Brandenburg, Phys. Rev. E **64**, 056405 (2001).
[37] A. Brandenburg, T. Kahniashvili, S. Mandal, A. Roper Pol, A. G. Tevzadze, and T. Vachaspati, arXiv:1710.01628.
[38] A. Brandenburg, K. Enqvist, and P. Olesen, Phys. Rev. D **54**, 1291 (1996).
[39] T. Vachaspati, arXiv:hep-ph/9405286.
[40] A. S. Monin and A. M. Yaglom, *Statistical Fluid Mechanics* (MIT Press, Cambridge, MA, 1975).
[41] R. Durrer and C. Caprini, J. Cosmol. Astropart. Phys. 11 (2003) 010.
[42] P. Huang, A. J. Long, and L. T. Wang, Phys. Rev. D **94**, 075008 (2016).
[43] J. R. Espinosa, T. Konstandin, and F. Riva, Nucl. Phys. **B854**, 592 (2012).
[44] J. Kozaczuk, S. Profumo, L. S. Haskins, and C. L. Wainwright, J. High Energy Phys. 01 (2015) 144.
[45] J. R. Espinosa, T. Konstandin, J. M. No, and G. Servant, J. Cosmol. Astropart. Phys. 06 (2010) 028.
[46] M. Kamionkowski, A. Kosowsky, and M. S. Turner, Phys. Rev. D **49**, 2837 (1994).
[47] A. Kosowsky, A. Mack, and T. Kahniashvili, Phys. Rev. D **66**, 024030 (2002).
[48] E. Witten, Phys. Rev. D **30**, 272 (1984).
[49] C. J. Hogan, Phys. Lett. B **133**, 172 (1983).
[50] D. Grasso and H. R. Rubinstein, Phys. Rep. **348**, 163 (2001).
[51] S. Candelaresi and A. Brandenburg, Phys. Rev. E **84**, 016406 (2011).
[52] V. Arnold, in *Vladimir I. Arnold—Collected Works* (Springer, Berlin, Heidelberg, 2014) Vol. 2, p. 357.
[53] H. K. Moffatt, J. Fluid Mech. **159**, 359 (1985).
[54] T. Kahniashvili, A. Brandenburg, A. G. Tevzadze, and B. Ratra, Phys. Rev. D **81**, 123002 (2010).
[55] A. Brandenburg and T. Kahniashvili, Phys. Rev. Lett. **118**, 055102 (2017).
[56] P. Olesen, Phys. Lett. B **398**, 321 (1997).
[57] A. D. Sakharov, Pis'ma Zh. Eksp. Teor. Fiz. **5**, 32 (1967) [JETP Lett. **5**, 24 (1967)][Usp. Fiz. Nauk **161**, 61 (1991)] [Sov. Phys. Usp. **34**, 392 (1991)].
[58] A. Brandenburg, T. Kahniashvili, and A. G. Tevzadze, Phys. Rev. Lett. **114**, 075001 (2015).
[59] P. A. Davidson, J. Fluid Mech. **663**, 268 (2010).
[60] C. D. Dermer, M. Cavadini, S. Razzaque, J. D. Finke, and B. Lott, Astrophys. J. **733**, L21 (2011).
[61] A. M. Taylor, I. Vovk, and A. Neronov, Astron. Astrophys. **529**, A144 (2011).
[62] A. Neronov and I. Vovk, Science **328**, 73 (2010).